Optics Letters

High-energy femtosecond amplifier-similariton Er-doped fiber oscillator

Kuan-Chen Chu, Hao-Yuan Jiang, and Shang-Da Yang*

Institute of Photonics Technologies, National Tsing Hua University, Hsinchu 30013, Taiwan
**Corresponding author: shangda@ee.nthu.edu.tw*

Received 5 August 2015; revised 16 October 2015; accepted 19 October 2015; posted 19 October 2015 (Doc. ID 247244); published 10 November 2015

We demonstrated high-energy femtosecond amplifier-similariton oscillators with predominant Er-doped fibers of normal dispersion. Stably mode-locked pulses of ∼3 ps, 33 nJ were produced at 720 mW pump power, while a double-pass grating pair of 36% efficiency compressed the pulses to 156 fs and 47 kW peak power (a new record). Broad mode-locked spectra supporting transform-limited pulsewidths down to 60 fs were obtained by adjusting the intracavity waveplates and filter. Continuous wave (CW) mode-locked pulses up to 53 nJ were generated by increasing the pump power to 1.5 W and by introducing significant spectral phase modulation via an intracavity pulse shaper. However, weak subpulses or pedestal could arise along with increased shot-to-shot fluctuation under this extreme operation mode.

OCIS codes: (060.2320) Fiber optics amplifiers and oscillators; (140.4050) Mode-locked lasers; (140.7090) Ultrafast lasers.

http://dx.doi.org/10.1364/OL.40.005319

Dissipative-soliton and similariton lasers enabled by nonlinear pulse propagation in normally dispersive fibers have improved the pulse energy of mode-locked fiber oscillators by more than 1 order of magnitude [1]. The maximum pulse energy of Yb-doped fiber oscillators has reached ∼1 μJ [2]. In contrast, Er-doped fibers (EDFs) are subject to lower doping concentration, narrower gain bandwidth, and smaller core (to achieve normal dispersion). The highest uncompressed pulse energies (compressed pulsewidths) were produced by dissipative-soliton lasers with 20 nJ (750 fs, [3]), 34 nJ (369 fs, [4]), and 38 nJ (700 fs, [5]), respectively. The corresponding peak powers (after compression) remain less than the 40 kW record (3.5 nJ, 70 fs) achieved by an amplifier-similariton laser [6]. Although EDF amplifier (EDFA) can further boost the pulse energy [7], it is subject to increased noise, complexity, and cost. In the applications of 3D microprinting, *in vivo* nonlinear microscopy [8], optical coherence tomography [9], EDF oscillators able to deliver tens of nJ pulse energy and ∼100 kW peak power would be sufficient and particularly attractive.

It has been recognized that amplifier-similariton lasers (made of long normally dispersive gain fiber and a filter) allow higher pulse energy and shorter pulse duration (thus stronger peak power) than the passive-similariton and dissipative-soliton counterparts [10]. In this regard, we previously demonstrated an amplifier-similariton oscillator with a cavity consisting of 17-m-long small-core EDF ($\beta_2 = 22.17\ \mathrm{ps}^2/\mathrm{km}$) and a programmable pulse shaper, producing 8.9 nJ (before compression), 268 fs and 6.2 kW (after compression) pulse at 320 mW pump power [11]. The extra spectral phase modulation added by the pulse shaper helped to suppress the nonlinear chirp and pedestal energy without incurring extra nonlinearity. In this contribution, we improved the pulse energy, compressed pulsewidth and peak power to 33 nJ, 156 fs and 47 kW (a new record) by increasing the EDF length (30 m) and pump power (720 mW). Over 100 kW peak power would be readily available by using an accessible high-efficiency (80%) grating pair compressor. Broad mode-locked spectra supporting transform-limited (TL) pulsewidths down to 60 fs were obtained by adjusting the intracavity waveplates and filter. Continuous wave (CW) mode-locked pulse energies up to 53 nJ were achieved by further increasing the pump power (1.5 W), the EDF length (40 m), and activating the spectral phase modulation via the intracavity pulse shaper at the price of energy leakage from the main pulse and increased shot-to-shot fluctuation.

Figure 1 shows the experiment setup. The gain medium was an EDFA (EDFA1, GIP Technology) comprised of cascaded EDF ($\beta_2 = 22.17\ \mathrm{ps}^2/\mathrm{km}$) and single-mode fiber (SMF, $\beta_2 = -21.94\ \mathrm{ps}^2/\mathrm{km}$) sections (1.7-m SMF, 6-m EDF, 1.2-m SMF, 24-m EDF, and 1.1-m SMF). The maximum pump power and corresponding total group delay dispersion (GDD) are 720 mW and 0.58 ps^2, respectively. For the highest output pulse energy, another EDFA2 (Alnair Labs) with 1.5 W pump power was used. It was made of a 40-m-long EDF ($\beta_2 = 14\ \mathrm{ps}^2/\mathrm{km}$) sandwiched between two 1-m-long SMF leads, contributing to a GDD of 0.52 ps^2. In contrast to the previous works [3–5], no dispersion compensating fiber was used in either of the two EDFAs to introduce a large amount of normal GDD. Saturable absorption was implemented by nonlinear polarization evolution (NPE) with waveplates and a polarization beam splitter. A slit or a liquid crystal spatial light modulator (SLM) was placed on the focal plane of a 4-f zero-dispersion compressor to achieve spectral filtering or programmable chirping to stabilize mode locking.

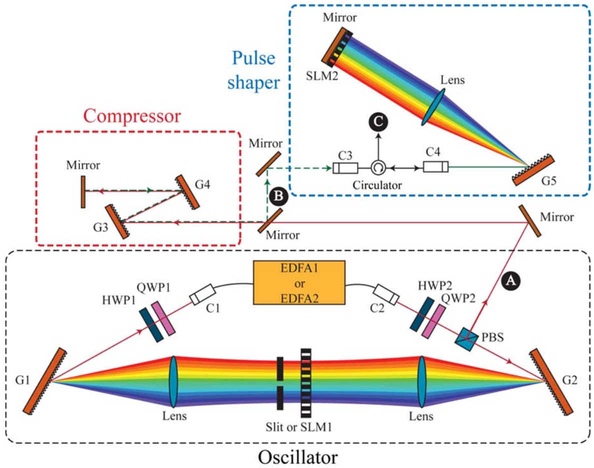

Fig. 1. Experiment setup. EDFA#, erbium doped fiber amplifier; HWP#, half-wave plate; QWP#, quarter-wave plate; PBS, polarization beam splitter; G#, grating; C#, collimator; SLM#, spatial light modulator. The solid and dashed lines in the compressor stand for beam paths at different heights.

By properly adjusting the waveplates and the filter passband (centered at 1563 nm and spanning 5.40 nm), we got a stably mode-locked spectrum [Fig. 2(a)] at the maximum pump power (720 mW) of EDFA1. The FWHM and rms bandwidth were 29 nm (3.4 THz) and 38 nm (4.6 THz), respectively. The rippled shape and smoother edges are signatures of amplifier-similariton pulses from the NPE output port [6,10,11], in contrast to the smoother shape and steeper edges of standard dissipative-soliton lasers [3–5]. The average power measured at Node A (Fig. 1) was 187 mW, corresponding to 33 nJ pulse energy (5.69 MHz repetition rate). Intensity autocorrelation (IA) trace of this uncompressed output pulse [inset, Fig. 2(b)] had a correlation width (FWHM) of 2.9 ps. The single-pulse and CW mode-locking operation was confirmed by satellite-free long-range (±200 ps) IA [Fig. 2(b)] and oscilloscope [Fig. 2(c)] traces, and the uniform envelope of the radio-frequency (RF) spectrum [inset, Fig. 2(d)]. The amplitude fluctuation and timing jitter calculated by the first harmonic [Fig. 2(d)] and the 35th harmonic of the RF spectrum were 0.19% and 4.56 ps, respectively.

To maximize the peak power and minimize the pulsewidth, the quadratic and higher-order spectral phase components of the pulse at Node A were sequentially compensated by a double-pass (thus spatial chirp-free) grating pair compressor and an extracavity Fourier transform pulse shaper (Fig. 1), with efficiencies of 36% and 18%, respectively. Once the pulse at Node C became TL, the residual spectral phase $\phi_{\mathrm{res}}(\lambda)$ at Node B could be determined by the conjugate phase modulation applied via the pulse shaper.

Figure 3(a) shows the originally measured $\phi_{\mathrm{res}}(\lambda)$ (solid) and its fifth-order polynomial fitting (dashed). The temporal intensity [inset, Fig. 3(b)] calculated by the measured power spectrum and fitted spectral phase corresponds to 73% pulse compression efficiency (the main pulse takes 73% energy), 156 fs pulsewidth (FWHM), and 47 kW peak power. The peak power is higher than the record (40 kW) reported in [6], and can become its 2.6 times (104 kW) if a grating compressor of the same (80%) efficiency is employed. The IA traces measured at Node B [solid, Fig. 3(b)] and Node C [solid, Fig. 3(c)] are in good agreement with the simulated counterparts [dashed, Figs 3(b) and 3(c)], proving the integrity of the measured $\phi_{\mathrm{res}}(\lambda)$.

The output spectrum of the oscillator could be flexibly manipulated by controlling the waveplates and filter passband. For example, the rms bandwidth increased from 38 to 60 nm [Fig. 4(a)] when the filter passband was centered at 1558 nm and 5.49 nm width. The average power measured at Node A (Fig. 1) dropped to 96 mW, corresponding to 17 nJ pulse energy. All the remaining characterizations were performed at Node C. The experimentally measured IA trace [solid, Fig. 4(b)] agreed well with the simulated one assuming TL

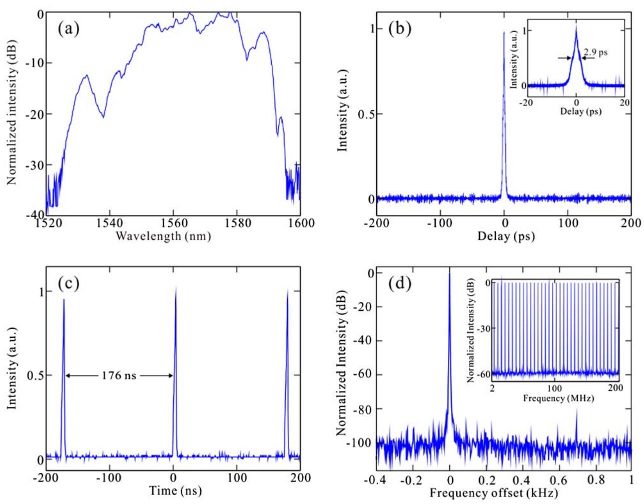

Fig. 2. Characterization results of the 33 nJ pulse train at Node A. (a) Power spectrum; (b) intensity autocorrelation (IA) traces over ±200 and ±20 ps (inset) delay ranges; (c) oscilloscope trace (recorder by using 50 GHz photodetector and 350 MHz oscilloscope); (d) RF spectrum centered at 5.69 MHz with 1 Hz resolution. Inset: RF spectrum spanning from 2 to 200 MHz with 10 kHz resolution.

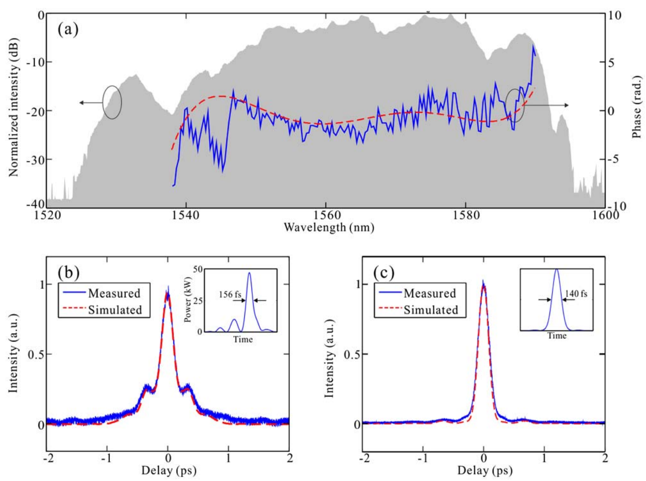

Fig. 3. Characterization results of the 33 nJ pulse trains at Nodes B and C. (a) Power spectrum (shaded), residual spectral phases at Node B obtained by the pulse shaper (solid) and fitting (dashed), respectively; (b) IA traces at Node B obtained by experiment (solid) and simulation (dashed). Inset: temporal intensity at Node B; (c) counterparts of (b) at Node C.

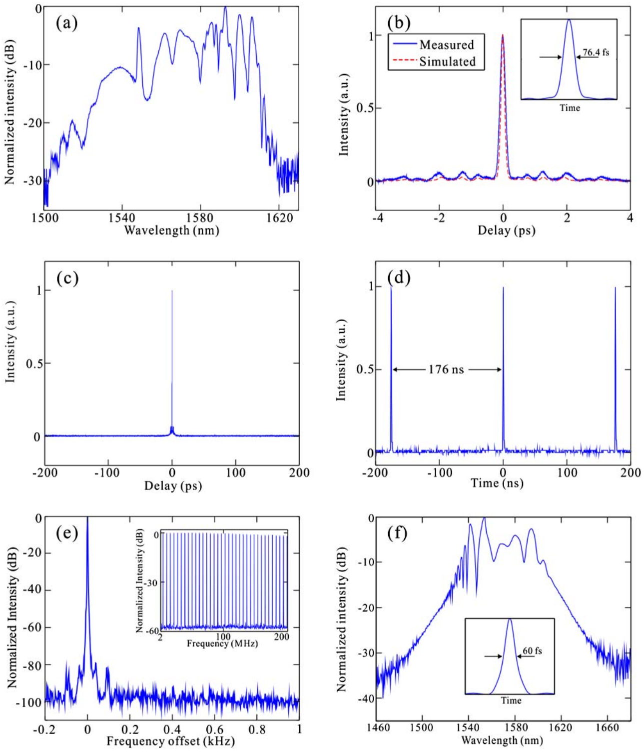

Fig. 4. Characterization results of the broadband pulses. (a) Power spectrum supporting a 76 fs TL pulse; (b) IA traces obtained by experiment at Node C (solid) and simulation assuming TL pulse (dashed), respectively. Inset: temporal intensity of the TL pulse; (c) IA trace at Node C measured over ±200 ps delay range; (d) oscilloscope trace; (e) RF spectrum centered at 5.69 MHz with 1 Hz resolution. Inset: RF spectrum spanning from 2 to 200 MHz with 10 kHz resolution; (f) power spectrum supporting a 60 fs TL pulse (inset).

pulse [dashed, Fig. 4(b)], verifying the nearly perfect dechirping enabled by the extracavity pulse shaper. The TL pulse [inset, Fig. 4(b)] had 76 fs width (FWHM) and 89% pulse compression efficiency. The single-pulse and CW mode-locking operation was confirmed by satellite-free long-range (±200 ps) IA [Fig. 4(c)] and oscilloscope [Fig. 4(d)] traces and the uniform envelope of the RF spectrum [inset, Fig. 4(e)]. The increased RF spectral pedestal [Fig. 4(e)], however, indicated a stronger shot-to-shot fluctuation of this broadband pulse train. The amplitude fluctuation and timing jitter calculated by the first harmonic and the 35th harmonic of the RF spectrum were 0.49% and 4.21 ps, respectively. Figure 4(f) shows the broadest mode-locked spectrum we managed to achieve by further adjusting the waveplates. The bandwidth supported 60 fs TL pulsewidth (FWHM), while the spectral wings exhibited even smoother edges. The oscillator worked on the verge of wave-breaking and only produced an even lower output power (77 mW).

In an attempt to investigate the maximum pulse energy that can be produced by amplifier-similariton oscillators, we replaced the gain medium by EDFA2 with doubled pump power (1.5 W) and a smaller repetition rate (4.50 MHz). In addition to adjusting the intracavity waveplates and slit, we gradually increased the third-order spectral phase modulation via the SLM placed before the slit to suppress wave-breaking until stable mode-locking was observed. Unlike the cases of EDFA1 and previous work [11], no stable mode-locking was obtained in the absence of the SLM. In one example, a stably mode-locked spectrum [Fig. 5(a)] with 238 mW average power was obtained at Node A when a third-order spectral phase with 8.02 ps^2 GDD and a cubic spectral phase coefficient of 5.98 ps^3 was added via the SLM. The corresponding pulse energy (53 nJ) exceeds the previous record (38 nJ [5]), and that of a recent amplifier-similariton oscillator (3.5 nJ, [6]) by 1.4 and 15 times, respectively. The oscilloscope trace [Fig. 5(b)] and long-range (±200 ps) IA trace [Fig. 5(c)] (measured at Node B) confirmed CW mode-locking and no extra main pulse in each repetition period. However, the latter exhibited a deep trench separating the main peak from the side bump and background, implying the presence of weak subpulses and/or broad pedestal at tens of picoseconds away from the main pulse. The RF spectrum had a more structured envelope [inset, Fig. 5(d)] and stronger pedestal [Fig. 5(d)] than those at lower energies [Figs 2(d) and 4(e)], supporting the above conjecture and indicating a degraded train stability. The odd features of the high-energy waveform could arise from the excessively long fiber cavity that is subject to noise burst [12] or noise-like multiple pulses [13]. The spectral stub around 1669 nm [Fig. 5(a)] coincides with the Raman-signal wavelength, implying the risk of soliton explosion where secondary pulse and irregular temporal waveform collapses could occur [14,15].

We demonstrated a stably mode-locked pulse train at 33 nJ energy emitted from an amplifier-similariton oscillator pumped at 720 mW. By using a double-pass grating pair compressor with 36% efficiency, we got 156 fs pulse duration and a record peak power of 47 kW. Over 100 kW peak power is readily available if a high-efficiency (80%) grating pair compressor is employed. By adjusting the waveplates and filter inside the cavity, the same setup can generate broad spectra with TL pulsewidths down to 60 fs. CW mode-locked pulses up to 53 nJ were generated by increasing the pump power to 1.5 W and by introducing significant spectral phase modulation via an intracavity pulse shaper at the cost of undesired subpulses and/or

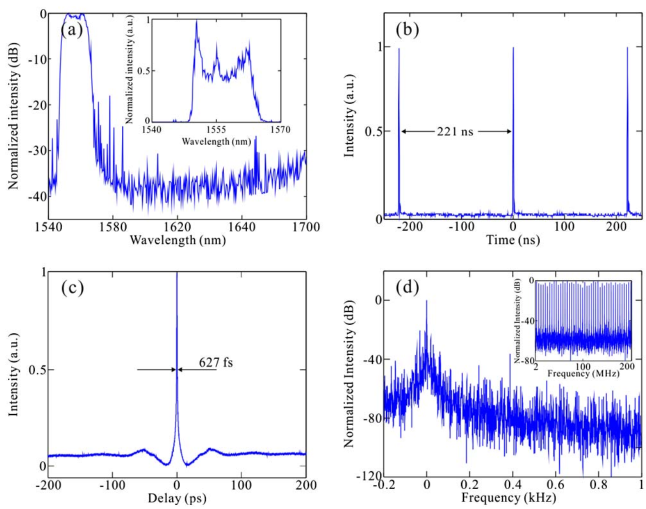

Fig. 5. (a) Power spectrum spanning over 1540–1700 nm. Inset: the zoom-in figure spanning over 1540–1570 nm in linear scale; (b) oscilloscope trace; (c) IA trace at Node B measured over ±200 ps; (d) RF spectrum centered at 4.50 MHz with 1 Hz resolution. Inset: RF spectrum spanning from 2 to 200 MHz with 10 kHz resolution.

broad pedestal. The cavity with a built-in programmable pulse shaper provides a useful platform to explore the rich phenomena of nonlinear dynamics [16]. To facilitate practical applications, the cavity design can be simplified by using fiber-optic polarization controllers and a polarization beam splitter. Further simplification is possible if the spectral filtering and extra chirping needed to stabilize mode-locking are known. In this case, the programmable intracavity pulse shaper (made of gratings, lenses, and SLM) can be replaced by a customized chirped mirror with compact size and low loss to introduce the static spectral modulation.

Funding. Industrial Technology Research Institute (ITRI), Taiwan (102A0116N6); Ministry of Science and Technology, Taiwan (MOST) (103-2218-E-007-010, 103-2218-E-007-010, 103-2221-E-007-056); National Tsing Hua University (NTHU) (104N2081E1).

Acknowledgment. We thank GIP Technology Corporation, Dr. C. B. Huang (NTHU), Dr. C. Fu (NTHU), and Dr. Y. S. Ku (ITRI) for customizing the EDFA1 and technical supports, respectively.

REFERENCES

1. F. W. Wise, A. Chong, and W. H. Renninger, Laser Photon. Rev. **2**, 58 (2008).
2. B. Ortaç, M. Baumgartl, J. Limpert, and A. Tünnermann, Opt. Lett. **34**, 1585 (2009).
3. N. B. Chichkov, K. Hausmann, D. Wandt, U. Morgner, J. Neumann, and D. Kracht, Opt. Lett. **35**, 2807 (2010).
4. H. Jeong, S. Y. Choi, F. Rotermund, Y.-H. Cha, D.-Y. Jeong, and D.-I. Yeom, Opt. Express **22**, 22667 (2014).
5. M. Tang, H. Wang, R. Becheker, J.-L. Oudar, D. Gaponov, T. Godin, and A. Hideur, Opt. Lett. **40**, 1414 (2015).
6. H. Liu, Z. Liu, E. S. Lamb, and F. Wise, Opt. Lett. **39**, 1019 (2014).
7. J. W. Nicholson, A. D. Yablon, P. S. Westbrook, K. S. Feder, and M. F. Yan, Opt. Express **12**, 3025 (2004).
8. N. G. Horton, K. Wang, D. Kobat, C. G. Clark, F. W. Wise, C. B. Schaffer, and C. Xu, Nat. Photonics **7**, 205 (2013).
9. H. Kawagoe, S. Ishida, M. Aramaki, Y. Sakakibara, E. Omoda, H. Kataura, and N. Nishizawa, Biomed. Opt. Express **5**, 932 (2014).
10. W. H. Renninger, A. Chong, and F. W. Wise, Phys. Rev. A **82**, 021805 (2010).
11. H.-W. Chen, C.-L. Tsai, L.-F. Yang, M.-H. Lin, K.-C. Chu, and S.-D. Yang, J. Lightwave Technol. **32**, 3277 (2014).
12. M. Horowitz and Y. Silberberg, IEEE Photon. Technol. Lett. **10**, 1389 (1998).
13. O. Pottiez, B. Ibarra-Escamilla, E. A. Kuzin, J. C. Hernández-García, A. González-García, and M. Durán-Sánchez, Laser Phys. **24**, 015103 (2014).
14. C. Aguergaray, A. Runge, M. Erkintalo, and N. G. R. Broderick, Opt. Lett. **38**, 2644 (2013).
15. A. F. J. Runge, N. G. R. Broderick, and M. Erkinyalo, Optica **2**, 36 (2015).
16. P. Grelu and N. Akhmediev, Nat. Photonics **6**, 84 (2012).